Flexibility-Aware System-on-Polymer (SoP): Concept to Prototype

Ujjwal Gupta, Jaehyun Park, Hitesh Joshi, and Umit Y. Ogras

Abstract—Mechanically flexible, printed, and stretchable electronics are gaining momentum. While rapid advancement is well underway at the device and circuit levels, researchers have yet to envision the system design in a flexible form. This paper introduces the concept of *System-on-Polymer (SoP)* based on flexible hybrid electronics (FHE) to combine the advantages of flexible electronics and traditional silicon technology. First, we formally define flexibility as a new design metric in addition to existing power, performance, and area metrics. Then, we present a novel optimization approach to place rigid components onto a flexible substrate while minimizing the loss in flexibility. We show that the optimal placement leads to as much as 5.7× enhancement in flexibility compared to a naïve placement. We confirm the accuracy of our models and optimization framework using a finite element method (FEM) simulator. Finally, we demonstrate the SoP concept using a concrete hardware prototype, and discuss the major challenges in the architecture and design of SoPs.

Index Terms—Flexible hybrid electronics, optimization, placement

1 Introduction

Bendable, rollable, conformal, or elastic circuits, commonly known as flexible electronics, are emerging as a promising alternative to conventional rigid circuits. Systems designed using flexible electronics can be lighter, thinner and less expensive to manufacture [37]. Hence, they can enable wearable systems, such as electronic shirts, ties, and fire-fighter jackets, as well as arbitrarily shaped objects like electronic labels [18]. Current examples of flexible electronics include displays [5], sensors [46], photovoltaic cells [58], batteries [30], simple micro-controllers, radio frequency integrated chip (RFIC) [1], and electronic paper [25].

Flexible electronics suffer severely from lower degrees of integration, limited performance and larger parameter variations compared to the state-of-the-art silicon technology, despite their huge potential in terms of new applications. For example, silicon technology offers 14 nm feature size with an operating frequency in the order of 2 GHz, whereas feature sizes of thin-film transistors (TFT) range from 8 $\mu\mathrm{m}$ to 50 $\mu\mathrm{m}$ [23] with frequencies hardly exceeding a few MHz [29]. While this huge capacity gap can be reduced by novel approaches, such as carbon-based semiconductors [7], [50], [55], flexible electronics are still far from implementing a full-fledged multiprocessor system-on-chip (SoC) with power and performance figures competitive with silicon technology. Consequently, the practical use of flexible electronics is limited to sensors and displays [44], [45].

Emerging *flexible hybrid electronics* can target the shortcomings of flexible electronics by integrating traditional rigid chips and printed electronics on a flexible substrate [9], [43]. This hybrid approach combines the processing and storage capabilities of rigid chips with the physical and cost benefits of flexible electronics. We propose using FHE to implement electronic systems on flexible substrates, as depicted in Fig. 1. Since the most common flexible substrates are plastic, polymer and paper, we coined the term SoP, which stands for *System-on-{Polymer, Plastic or Paper}* [21]. The idea behind this hybrid approach is to use rigid chips where high performance, processing and storage capabilities are needed, while reverting to flexible electronics for everything else to maintain the benefits of flexibility. By integrating flexible display, sensors, and battery with conventional chips, this generic architecture allows for a wide spectrum of systems, ranging from simple internet-of-things (IoT) devices [32], [56] to complex mobile platforms like smartphones [3]. Therefore, SoP architectures have the potential to transform personal computing by enabling arbitrarily shaped wearable systems that are not limited to desks, laps or hands.

The fundamental difference between SoPs and SoCs is the physical flexibility. Since flexible electronics exhibit poor performance and scalability [25], [38], a large number of rigid chips are preferred to boost processing power. However, doing so would also undermine the advantages of flexibility. This aggravates existing communication, reliability, power and thermal challenges. FHE exhibits an inherent design trade-off between flexibility and computational efficiency (more rigid chips), as illustrated in Fig. 2. Therefore, designing SoP architectures, such as the one illustrated in Fig. 1, requires a formal and quantitative definition of flexibility as a new metric.

This paper presents an analytical *flexibility* model as a new design metric in addition to traditional area, power, and performance metrics. Using this model, we construct an optimization approach to place rigid chips onto flexible substrates to maximize the flexibility. We show that the optimal placement leads to as much as 5.7× increase in

• *The authors are with the School of Electrical, Computer, and Energy Engineering, Arizona State University, Tempe, AZ 85281. E-mail: {ujjwal, jpark244, hjoshi5, umit}@asu.edu.*

Manuscript received 4 Feb. 2016; revised 5 Nov. 2016; accepted 13 Nov. 2016. Date of publication 8 Dec. 2016; date of current version 16 Mar. 2017. Recommended for acceptance by S. Bhunia. For information on obtaining reprints of this article, please send e-mail to: reprints@ieee.org, and reference the Digital Object Identifier below. Digital Object Identifier no. 10.1109/TMSCS.2016.2637345

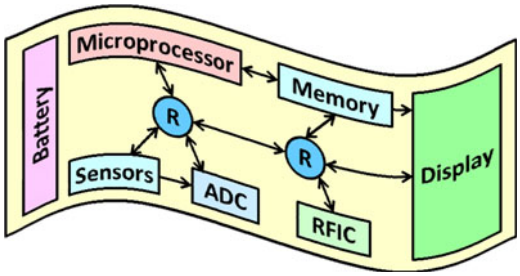

Fig. 1. A SoP with battery, sensors, analog-to-digital converter (ADC), microprocessor, memory, RFIC, and display connected by flexible routers.

flexibility compared to a naïve placement. We evaluate the accuracy of the analytical models and effectiveness of the proposed optimization approach using finite element method (FEM) simulations [51]. Finally, we demonstrate the SoP concept by presenting one of the first FHE prototypes implemented on a Polyimide substrate.

The major contributions of this paper are as follows:

- Defining flexibility as a new design metric for SoP architectures,
- A methodology for the optimal placement of rigid chips on a flexible substrate to maximize flexibility,
- A concrete SoP prototype for motion processing, and experimental evaluation of a flexible antenna as a function of bending.

The rest of this paper is organized as follows: Section 2 presents an overview of related research. Section 3 presents the proposed flexibility model and optimal placement approach. Section 4 presents the FEM simulation results that validate the proposed flexibility model, and discusses the optimization results. Section 5 presents a concrete SoP prototype and the experimental results. Section 6 discusses the architectural challenges and potential research directions. Finally, Section 7 presents the conclusions drawn from this paper.

2 Related Research

Several institutions have recently demonstrated the feasibility of flexible electronics [1], [5], [20]. For example, flexible 8-bit microcontroller (MCU), ADC, and RFIC have been successfully manufactured using TowerJazz CS18 PD-SOI CMOS process. This approach to manufacturing flexible electronics uses lower complementary metal-oxide semiconductor (CMOS) process technology nodes, then converts the circuit to flexible form-factor [1]. Fully flexible asynchronous MCU and static random-access memory (SRAM) have also been developed using low-temperature poly-silicon TFT technology [16], [28]. Similarly, integrated programmable logic circuits have been recently demonstrated in [47].

Prior research on electrical properties of fully flexible circuits—implemented using various technologies—has been demonstrated with the help of ring oscillators [12], [13], [27], [54], [57]. The work presented in [34] proposed a placement technique for TFTs by taking bending into account. In contrast, our approach is at the macro level, and targets FHE system design using rigid components on a flexible substrate. We refer the reader to [25] for a comprehensive overview of flexible electronics and associated design automation challenges.

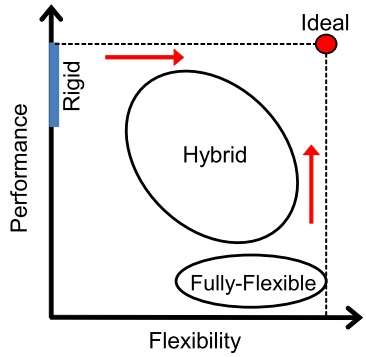

Fig. 2. Motivation for flexible hybrid electronics.

Since flexible components have significantly lower performance compared to CMOS technology, using flexible hybrid electronics is encouraged by national research agencies [49]. Integration of CMOS devices on flexible substrates has recently been demonstrated at research centers including the ASU Flexible Display Center [20], [48], as well as in the industry [1] and academia [22]. However, only a handful of studies addressed the design of hybrid systems to date. Hu et al. [22] have recently presented a hybrid self-powered system that combines sensing capabilities and long-range interconnects of large area flexible electronics with the processing advantages of CMOS chips. In [36], the authors presented interface circuits between flexible electronics and CMOS chips using capacitively-coupled signals.

The early examples of FHE systems are critical milestones that show the feasibility of transforming computer systems via SoPs. However, the current technology mainly aims at individual devices [38]. Furthermore, there are no proposed solutions for the systematic design of FHE systems. Towards developing a complete methodology, this paper takes a system-level view and considers optimal integration of many macro-resources such as processor, display and sensors. We quantify flexibility as a new metric, and develop an optimal placement approach.

3 Optimum Placement of Rigid Components on Flexible Substrates

Physical flexibility is a new design dimension that has not been considered by computer system designers so far. In order to incorporate flexibility in the design process, we quantify the maximum deflection of a flexible substrate as a measure of flexibility. This formalism enables us to treat flexibility as a *measurable* design metric. For example, it becomes possible to minimize the loss of flexibility under power/performance constraints, or impose a constraint on the loss in flexibility due to a rigid component. Then, we develop a design methodology for *optimally* placing rigid components on a flexible substrate with the objective of maximizing flexibility.

3.1 Flexibility Metric for Flexible Hybrid Systems

Consider a simple flexible hybrid system with one rigid component placed over a flexible substrate, as illustrated in Fig. 3. We assume that the flexible substrate is a flat, homogenous isotropic material with uniform thickness. There are four pairs of uniformly distributed major bending forces

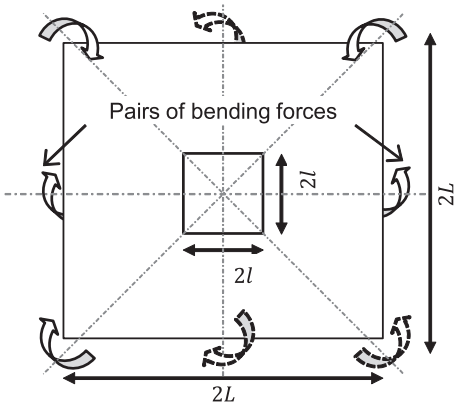

Fig. 3. A simple flexible hybrid system with one rigid component mounted over a large flexible substrate. Four possible uniform bending-force pairs are shown.

that can be applied on the flexible substrate. All forces are normal to the plane of the flexible surface and uniformly distributed along the bending axis. We use the sum of the maximum deflection on each side of the rigid component as the flexibility metric.

To analyze the impact of the relative size of a rigid component on flexibility, we consider a rigid chip of dimension $2l \times 2l$ mounted over flexible substrate of dimension $2L \times 2L$, as shown in Fig. 3. We model this flexible hybrid system using two cantilever beams. First, the side-view of the flexible substrate alone and equivalent forces with pivot point are shown in Fig. 4a. Then, the corresponding view for the flexible hybrid system is shown in Fig. 4b. We analyze the deflection at the sides as two separate cantilever beams when the rigid chip is placed at the center, as shown in Fig. 4c. In reality, the shear stress at the pivot will make some difference in the analysis of the pivoted beam and cantilever, but it is marginal and can be neglected due to the thin flexible substrate. Cantilever beams without and with the rigid component are shown in Figs. 4d and 4e, respectively. These two figures illustrate that the rigid component decreases the effective length of the cantilever beam.

We can express the maximum deflection in a cantilever beam as a function of the uniformly distributed force P applied at one end (point force), modulus of elasticity E, and moment of area I as $\delta_{\max} = \frac{L^3 P}{3EI}$ [4]. Hence, the maximum deflection in the fully flexible (δ_{FF}), and flexible hybrid (δ_{FH}) systems shown in Figs. 4d and 4e are given by

$$\delta_{FF} = \frac{L^3 P_{\max}}{3EI} \quad \text{and} \quad \delta_{FH} = \frac{(L-l)^3 P_{\max}}{3EI}, \tag{1}$$

where $P_{\max}$ is the maximum force the substrate can sustain before breaking. If the contact (e.g., soldering) between the rigid component and flexible substrate is weaker than the flexible substrate, $P_{\max}$ will be smaller than the actual material breaking force. Using Equation (1), we can compute the reduction in deflection using as

$$\text{Deflection Loss} = \frac{\delta_{FF} - \delta_{FH}}{\delta_{FF}} = \frac{L^3 - (L-l)^3}{L^3}. \tag{2}$$

Flexibility Loss. The loss in flexibility is plotted in Fig. 5 using Equation (2) as a function of the ratio between the

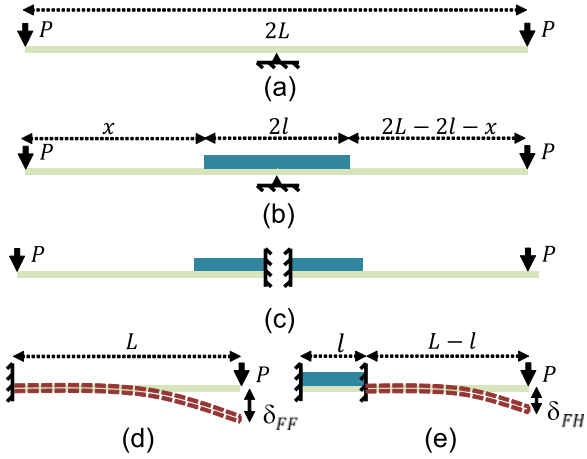

Fig. 4. Procedure for modeling the flexible hybrid system as a cantilever beam problem with special case, $x = L - l$.

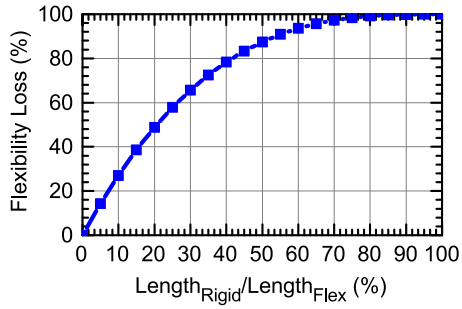

Fig. 5. The flexibility loss in flexible hybrid system compared to fully flexible system with one chip.

lengths of the rigid component and the flexible substrate. When the rigid component is 20 percent in length compared to the flexible portion, the flexibility loss is 45 percent. We observe that increasing the area of the rigid chip quickly diminishes the flexibility. Since moving more functionality to the rigid chips implies higher performance and larger rigid area, Equation (1) enables the analysis of the tradeoff between the new flexibility metric and traditional metrics such as area and performance.

So far, we have considered the scenario where the rigid chip is placed at the center for illustration purposes. If the rigid chip is placed at an arbitrary location x from one end point, as depicted in Fig. 4b, then the flexibility of the flexible hybrid system can be found as

$$\delta_{FH} = \frac{x^3 P_{\max}}{3EI} + \frac{(2L - 2l - x)^3 P_{\max}}{3EI}. \tag{3}$$

3.2 Flexibility Model with Multiple Rigid Chips

Suppose that N rigid chips need to be placed on an $H \times L$ substrate. Let h_i be the height, l_i be the length, and (x_i, y_i) be the lower left corner coordinates of the ith chip. Any given pair of chips should not overlap at least in one dimension to obtain a valid placement. For example, if two chips *do not* overlap along the x-axis, an overlap along the y-axis is allowed, as illustrated in Fig. 6. Therefore, we start off with a placement along one dimension by considering the *non-overlapping* and *overlapping* scenarios separately.

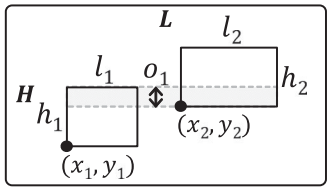

Fig. 6. A valid placement with overlap along the y-axis.

Non-Overlapping Placement. Without loss of generality, assume that the rigid chips are ordered such that $x_i < x_j \Rightarrow i < j$. If the rigid chips are non-overlapping, the flexibility model given in Equation (3) can be extended to a function of N variables $\delta(\boldsymbol{x}) = \delta(x_1, x_2, \ldots, x_N) : \mathbb{R}^N \rightarrow \mathbb{R}$ as

$$\delta(\boldsymbol{x}) = \frac{P_{\max}}{3EI}\left[x_1^3 + \sum_{i=1}^{N-1}\left(x_{i+1} - (x_i + l_i)\right)^3 \; + \; \left(L - (x_N + l_N)\right)^3\right]. \tag{4}$$

The first term inside the square bracket (i.e., x_1^3) is the deflection due to the flexible region between the side $x = 0$ and the first rigid chip. Similarly, the last term gives the deflection due to the flexible region between the opposite side and the Nth chip. Finally, the intermediate terms represent the contributions due to the spacing between the rest of the rigid chips.

Overlapping Placement. If the rigid chips can overlap, we assume $\min_{1 \le i \le N} x_i = x_1$, i.e., the index of the rigid chip with the smallest x-coordinate is 1. The rest of the chips are ordered such that $(x_i + l_i) \le (x_j + l_j) \Rightarrow i < j$. That is, the ordering is with respect to the x-coordinate of the right side. Let o_i, $1 \le i < N$ be the overlap between the ith and $(i+1)$th rigid chip. Since the overlap between any pair of chips cannot exceed the length of the shorter one, we can write $0 \le o_i \le \min(l_i, l_{i+1})$, $1 \le i < N$. Using this definition, we introduce the following change in the variable to represent the x-coordinate of the rigid chips: $x_{i+1} = x_i + l_i - o_i, 1 \le i < N$. This enables us to express the coordinates as

$$\begin{aligned} x_2 &= x_1 + l_1 - o_1 \\ x_3 &= x_2 + l_2 - o_2 = x_1 + (l_1 + l_2) - (o_1 + o_2) \\ &\cdots \quad \cdots \\ x_N &= x_1 + \sum_{i=1}^{N-1} l_i - \sum_{i=1}^{N-1} o_i. \end{aligned} \tag{5}$$

Using these expressions, the flexibility model for N rigid chips that can overlap can be written as a function of N variables $\delta(x_1, \boldsymbol{o}) = \delta(x_1, o_1, o_2, \ldots, o_{N-1}) : \mathbb{R}^N \rightarrow \mathbb{R}$

$$\delta(x_1, \boldsymbol{o}) = \frac{P_{\max}}{3EI}\left[x_1^3 + \left(L - \left(x_1 + \sum_{i=1}^{N} l_i - \sum_{i=1}^{N-1} o_i\right)\right)^3\right]. \tag{6}$$

Similar to the non-overlapping case, the first term inside the square bracket is the deflection due to the flexible region between the side $x = 0$ and the first rigid chip, while the last term gives the deflection due to the flexible region between the opposite side and the Nth chip. The intermediate terms vanish since the rigid chips have non-zero overlap.

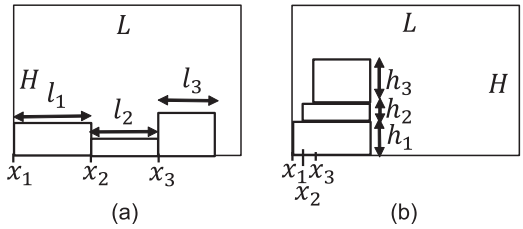

Fig. 7. Two sample instances of optimal placements for (a) non-overlapping and (b) overlapping in the x-dimension.

3.3 Optimal Placement along One Dimension

In this section, we present a theorem that specifies the optimal placement along the x-dimension using Equations (4) and (6). We will use this result to develop a methodology to place multiple rigid chips on a 2D substrate to maximize the flexibility.

Theorem 1. *Consider the placement of N rigid chips along one dimension (e.g., x-axis as shown in Fig. 4).*

1) If the rigid chips are not allowed to overlap, *the flexibility is maximized when all the chips are placed side by side (i.e., they form a contiguous region), on either side of the substrate, as illustrated in Fig. 7a. The maximum flexibility in this case is given as*

$$\delta_{\text{nonoverlapping}} = \frac{P_{\max}}{3EI}\left(L - \sum_{i=1}^{N} l_i\right)^3. \tag{7}$$

2) If the rigid chips can overlap, *the flexibility is maximized if the chips are placed on either side, and the overlap between each pair is maximum, as illustrated in Fig. 7b. The maximum flexibility in this case is given as*

$$\delta_{\text{overlapping}} = \frac{P_{\max}}{3EI}\left(L - \max_{1 \le i \le N} l_i\right)^3. \tag{8}$$

The proof of this theorem is presented in the Appendix.

3.4 Optimal Placement on a Flexible 2D Substrate

An important optimization criterion for 2D placement is the bending axis. For instance, horizontal bending is the primary concern in a wearable device in the form of a wristband. In general, horizontal, vertical, or diagonal bending, or even a combination thereof might be considered, depending on the target application.

Given the optimization goal, the theorem presented in Section 3.3 can be utilized within an algorithm to place multiple rigid chips on a 2D flexible substrate. The simplest solution would be an iterative heuristic that can place the rigid chips one by one so as to maximize the flexibility criterion at each step. More precisely, it can first place the next rigid component to form a contiguous region with *no overlap* along the x-axis and *overlap* along the y-axis. Then, it can compare this solution to the placement with *overlap* along the x-axis and *no overlap* along the y-axis. In this way, multiple chips can be sorted and placed iteratively.

A better approach would employ a more thorough backtracking algorithm, such as a depth first search [52], to

perform a global search. However, the combinatorial nature of an exhaustive search can quickly increase the complexity when the number of rigid chips and bending scenarios increase. Moreover, Theorem 1 gives the maximum flexibility for a fixed orientation. Therefore, the results of Theorem 1 alone will not give a global optimum in 2D, unless all ICs are of square shape or an exhaustive search is also performed for each possible orientation. To solve this problem, we propose an optimization method based on the Theorem 1.

In general, Theorem 1 indicates that the rigid chips should be packed to form a contiguous region, and placed on the side of the substrate parallel to the bending axis. Since packing the chips densely also reduces the interconnect length, we propose first packing the rigid chips into the smallest bounding-box *with a soft aspect ratio* using existing floorplanning techniques [2], [17]. Then, we define the bounding-box as the rigid area, as shown in Fig. 8. Our objective is to find the *optimal placement*, *aspect ratio* and *orientation* of the bounding-box as a function of the bending axis.

The geometric representation of a generic problem instance is shown in Fig. 8. Consider a flexible substrate $ABCD$, with the coordinates $A(0,0)$, $B(L,0)$, $C(L,H)$ and $D(0,H)$, respectively. The bounding-box $pqrs$ is placed with an arbitrary orientation angle θ with respect to the horizontal side of flexible substrate. The area of the bounding-box B_A is fixed, while the length l and height h are free variables where $B_A = l \times h$. Let the coordinates of point r be (x_r, y_r), then the coordinates of points s, p and q can be written as

$$(x_s, y_s) \equiv (x_r + h\cos\theta, y_r + h\sin\theta), \tag{9}$$

$$(x_p, y_p) \equiv (x_r + d\cos(\theta+\phi), y_r + d\sin(\theta+\phi)), \tag{10}$$

$$(x_q, y_q) \equiv (x_r + l\cos(\theta+\pi/2), y_r + l\sin(\theta+\pi/2)), \tag{11}$$

where $\phi = \tan^{-1}(l/h)$ and $d = \sqrt{l^2+h^2}$.

The flexible substrate can be bent across an arbitrary bending axis such as a_1 and a_2 shown in Fig. 8. For example, when the bending angle β (the angle between a_2 and x-axis) is zero, the substrate is bent horizontally, i.e., along the x-axis. Likewise, $\beta = \pi/2$ implies vertical bending along the y-axis. We consider uniform bending all throughout the flexible substrate, and model the system using cantilever beams. Since maximum deflection is proportional to the cube of length (Equation (1)), the longest cantilever beam will give the largest deflection for a given amount of force applied. For example, consider the two cantilever beam models, $|\mathrm{Am}|$ and $|\mathrm{Cn}|$ shown in Fig. 8. These cantilever beams are perpendicular to the two axes a_1 and a_2 and represent the longest length out of all other possible cantilevers. $|\mathrm{Am}|$ and $|\mathrm{Cn}|$ can be expressed as

$$|\mathrm{Am}| = x_r\sin\beta + y_r\cos\beta \tag{12}$$

$$|\mathrm{Cn}| = (L - x_r - d\cos(\theta+\phi))\sin\beta + (L - y_r - d\sin(\theta+\phi))\cos\beta. \tag{13}$$

In general, the flexibility can be written as the sum of deflections of these two cantilever beams

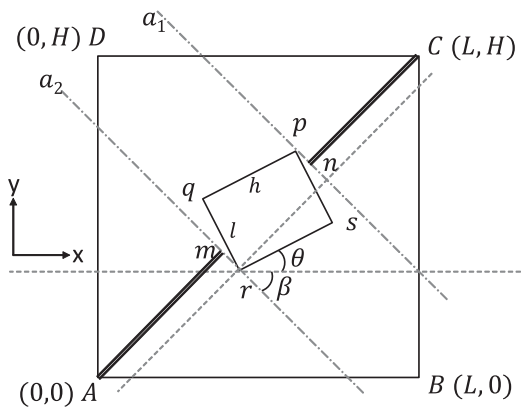

Fig. 8. Geometric illustration of an arbitrary bounding-box $pqrs$ with orientation θ over a flexible substrate $ABCD$ is shown. The bending axes a_1 and a_2 are parallel and equivalent to any other bending axis at an angle β and not intersecting the bounding-box region. $|\mathrm{Am}|$ and $|\mathrm{Cn}|$ are the lengths of cantilever beams.

$$\delta(x_r, y_r, \theta, \beta, l, h) = \frac{P_{max}}{3EI}\Big[(x_r\sin\beta + y_r\cos\beta)^3 + \big((L - x_r - d\cos(\theta+\phi))\sin\beta + (L - y_r - d\sin(\theta+\phi))\cos\beta\big)^3\Big]. \tag{14}$$

Equation (14) gives the flexibility for an arbitrary bending axis with angle β. Therefore, we can find the optimum dimensions l and h, orientation θ, and location (x_r, y_r) for the rigid bounding-box as a function of β. Depending on the usage scenario, we may want to bend the flexible substrate along multiple axes. For example, one might co-optimize for both horizontal and vertical bending instead of considering only one of them. Therefore, we define a set of bending angles, $\boldsymbol{\beta} = [\beta_1, \beta_2, \beta_3, \ldots, \beta_n]$ with corresponding relative importance $\boldsymbol{w} = [w_1, w_2, w_3, \ldots, w_n]$. As a result, we can define the objective function as a weighted sum of flexibility at different bending angles

$$\Delta(x_r, y_r, \theta, l, h, \boldsymbol{\beta}, \boldsymbol{w}) = \sum_{i=1}^{N} w_i \times \delta_i(x_r, y_r, \theta, \beta_i, l, h). \tag{15}$$

Our goal is to maximize the flexibility within the geometric constraints. This can be expressed using a nonlinear optimization problem as follows:

$$\begin{aligned} \text{maximize} \quad & \Delta(x_r, y_r, \theta, l, h, \boldsymbol{\beta}, \boldsymbol{w}) \\ \text{subject to} \quad & g_c : 0 \le x_p, x_q, x_r, x_s \le L, 0 \le y_p, y_q, y_r, y_s \le H, \\ & g_\beta : 0 \le \boldsymbol{\beta} \le \boldsymbol{\pi/2}, \\ & g_\theta : -\min(\boldsymbol{\beta}) \le \theta \le -\max(\boldsymbol{\beta}) + \pi/2, \\ & g_l : l \ge L_{\min},\ g_h : h \ge H_{\min} \\ & \text{Area of bounding-box} : B_A = l \times h, \\ & \sum_{i=1}^{N} w_i = 1,\ w_i \ge 0\ \forall i. \end{aligned} \tag{16}$$

The first inequality ensures that the bounding-box $pqrs$ remains within the flexible substrate boundary, while the second one constrains the bending angle g_β to the interval $[0, \pi/2]$. Similarly, g_θ constrains θ with respect to the

maximum and minimum β values. The constraints g_β and g_θ avoid symmetric solutions. We also have constraints for the area B_A, minimum length g_l, and minimum height g_h of the bounding-box. Finally, the weight of all bending angles sum to one, and all quantities except θ remain positive throughout the optimization.

System designers may want to pre-specify flexible only regions on the substrate where no rigid chips can be placed. For example, consider an arbitrarily shaped flexible-only region R_{FF} as an input to the optimization framework. The bounding-box region R_{BB} should be placed such that it does not intersect the flexible region R_{FF}, i.e., $R_{FF} \cap R_{BB} = \phi$. The separation between the two regions can be achieved by adding more constraints to the optimization formulation given in Equation (16). In particular, Linear Discriminant Analysis [6] can be used to check for the condition of existence of an affine transformation $f(x,y) = \mathbf{a}^T \begin{bmatrix} x \\ y \end{bmatrix} - b : \mathbb{R}^2 \rightarrow \mathbb{R}$ between the two regions

$$\begin{aligned} \mathbf{a}^T \mathbf{p_R} - b \geq t, \quad \mathbf{p_R} \in R_{FF} \\ \mathbf{a}^T \mathbf{q_R} - b \leq -t, \quad \mathbf{q_R} \in R_{BB}, \end{aligned} \tag{17}$$

where t is the margin between the affine transformation and the two regions R_{FF} and R_{BB}. If $\mathbf{a}$ and b exist for a given R_{FF} and R_{BB}, then the regions do not overlap and the bounding-box placement is valid. Therefore, with these constraints, the placement approach can avoid certain predefined flexible regions.

4 FEM Validation and Optimization Results

In this section, we first present the FEM simulation results to validate the accuracy of our flexibility metric. Then, we discuss optimization results obtained by solving the nonlinear program given in Equation (16).

4.1 Flexibility Model Validation

Simulation is an important component of electronic system design flows since it provides a trade-off between accuracy and speed. In our context, we have to validate the accuracy of the second order flexibility model given in Equation (1), before employing it for optimization. This validation can serve as a strong basis for FHE optimization approaches, such as our placement technique, that utilize the proposed flexibility model. We utilized COMSOL [10] multi-physics software to perform FEM simulations, since it enables the realistic study of multiple physical phenomena such as electrical inputs and structural deformations.

As the first step to validate the proposed flexibility model, we built the substrate and bounding-box geometry shown in Fig. 4e. We chose a Polyimide substrate since it is widely used in industry [14]. The output of FEM simulations and the analytical solution from Equation (1) are plotted in Fig. 9. The average percentage error between our analysis and FEM simulations is 2.0 percent. Moreover, the deflection of the SoP decreases with increasing size of the rigid bounding-box, as expected. The results show that our deflection model is highly representative of the real behavior. Therefore, it can be employed by other researchers to develop FHE optimization techniques. Furthermore, this simulation setup enables us to model a large set of real-life scenarios.

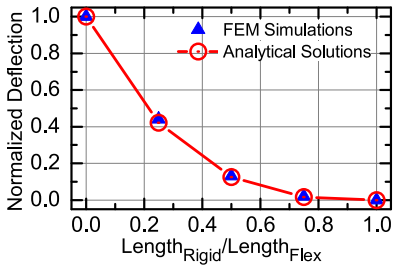

Fig. 9. Normalized deflection comparison between FEM simulations and analytical model given in Equation (3).

4.2 Optimization Results

We solved the general optimization problem given by Equation (16) using numerical techniques in Matlab for 10 units$\times$ 10 units flexible substrate and a bounding-box with area $B_A = 4$ units^2. We also derived the analytical solution for special cases $\beta = 0$ and $\beta = \pi/2$ for validation purposes. Since the most common bending angles are horizontal, vertical and along the diagonal, we set $\boldsymbol{\beta} = [0, \pi/4, \pi/2]$ to analyze the optimal placements.

In Fig. 10, the gray regions with dashed boundaries show the optimal bounding-box *regions* obtained by solving Equation (16). As a concrete placement example, the red box with solid boundaries is a particular instance of the solution to the optimization problem given by Equation (16). Fig. 10a shows the optimal placement under horizontal bending ($\boldsymbol{w} = [1, 0, 0]$). The optimal orientation is $\theta = 0$, while the dimension of the bounding-box is 4×1. This implies that the height of the optimal bounding-box comes out to be equal to the constraint, $H_{\min} = 1$. That is, the orientation is parallel to the bending axis and the dimension perpendicular to the bending axis is minimized as expected. Furthermore, we observed that the bounding-box can be placed on either side. This makes sense since the maximum displacement depends on the cube of the distance from the side, which is maximized when the bounding-box touches either side. Similarly, for vertical bending ($\boldsymbol{w} = [0, 0, 1]$), the optimal orientation is $\theta = -\pi/2$, the dimension of bounding-box is 4×1, and the placement is either on $x_r = 0$ or $x_r = 9$, as shown in Fig. 10b. When the bending is along the diagonal ($\boldsymbol{w} = [0, 1, 0]$), as shown in Fig. 10c, the orientation is $\theta = \pi/4$, as expected. We also note that the optimal dimensions are 1.41×2.83, which is non-trivial unlike the previous cases, while the placement was on either corner.

More complex scenarios with multiple bending angles are shown in Figs. 10d, 10e, 10f, 10g, and 10h. For vertical and horizontal bending together ($\boldsymbol{w} = [0.5, 0, 0.5]$), the output is $\theta = 0$, dimension of bounding-box is 2×2, and possible locations are $(0,0), (0,8), (8,0)$, and $(8,8)$, as shown in Fig. 10d. Note that the result is the same irrespective of any amount of additional diagonal bending, as shown in Fig. 10h. The results with $\boldsymbol{w} = [0.25, 0, 0.75]$ and $\boldsymbol{w} = [0.75, 0, 0.25]$, shown in Figs. 10e and 10f are similar to Figs. 10b and 10a, respectively. However, only the corners are optimal. For strong diagonal and vertical bending ($\boldsymbol{w} = [0, 0.75, 0.25]$), the result is similar to Fig. 10c, but has slightly different dimensions of bounding-box (1.46×2.73) and possible location $(0, 1.93)$.

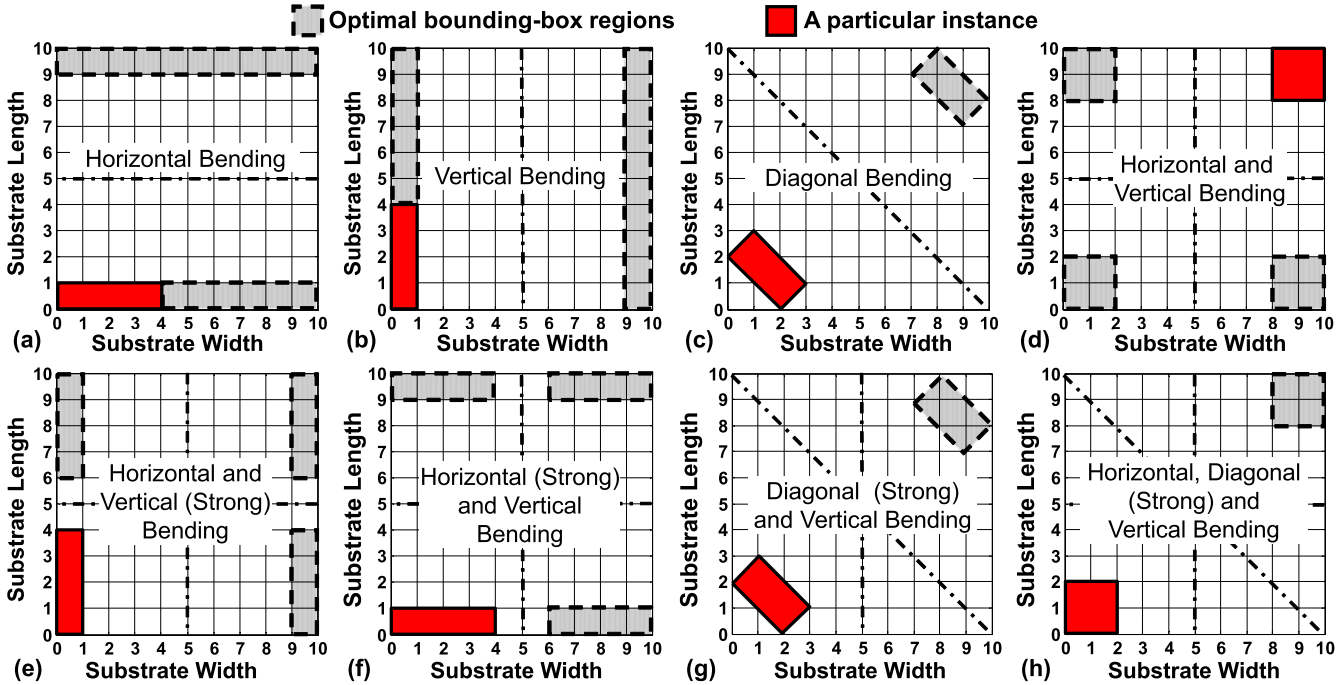

Fig. 10. Optimal bounding-box regions for the flexible hybrid system.

The tendency is to move the bounding-box towards the corners of the flexible substrate.

A naïve approach to place the bounding-box on the substrate could be at the center with dimensions 2×2, similar to the placement in Fig. 3. The flexibility comparison of the naïve approach versus the result of the optimized placement is shown in Table 1. On average, the optimal solution gives $4.58\times$ gain in flexibility. These results show substantial improvements in flexibility and signify the importance of optimal placement for wearable computing system design.

4.3 Validation of the Optimization Results

Once the accuracy of the flexibility model was established, we performed FEM simulations to validate the proposed optimum placement approach. To achieve this, we simulated all the bending scenarios considered in Fig. 10, and placed the bounding-box on the center of the substrate.

TABLE 1
The Gains in Flexibility Are Shown by Placing the Bounding-Box Optimally (Δ^*) as Opposed to Naïve Placing it at the Center (Δ_{center}) of the Substrate with Dimensions $10\ \text{cm} \times 10\ \text{cm} \times 300\ \mu\text{m}$, Elasticity $E = 7.95\ \text{GPa}$, and an Applied Force of $100\ \text{N/m}^2$

Fig. 10 index	Weight Vector			Max. Deflection (mm)		Gain in Flexibility
	W_0	$W_{\pi/4}$	$W_{\pi/2}$	Δ_{center}	Δ^*	
(a)	1.00	0.00	0.00	0.06	0.35	5.69 ×
(b)	0.00	0.00	1.00	0.06	0.35	5.69 ×
(c)	0.00	1.00	0.00	0.25	0.99	4.00 ×
(d)	0.50	0.00	0.50	0.06	0.25	4.00 ×
(e)	0.25	0.00	0.75	0.06	0.29	4.69 ×
(f)	0.75	0.00	0.25	0.06	0.29	4.69 ×
(g)	0.00	0.75	0.25	0.20	0.79	3.91 ×
(h)	0.20	0.60	0.20	0.17	0.69	4.00 ×

For example, Figs. 11a and 11b show the cases when the bounding-box is on the center and on the left hand side of the substrate, respectively. In agreement with the analytical results, placing the bounding-box on the side delivered $5.81\times$ improvement in flexibility over placing it on the center. Fig. 12 compares the FEM simulation results and analytical solutions for each of the bending scenarios shown in Fig. 10. The analytical model exhibited high fidelity across all the scenarios with horizontal and vertical bending. More precisely, the mean absolute percentage error between the flexibility of analytical and FEM simulation results was 5.9 percent.

5 System on Polymer Prototype

To demonstrate the feasibility of SoP architectures, we designed and manufactured a hardware prototype as an

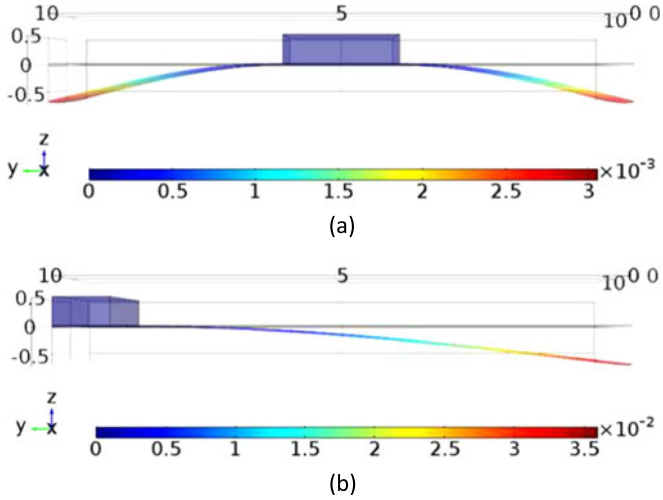

Fig. 11. The cross-sectional view of the COMSOL model when the bounding-box is at the (a) center and (b) side.

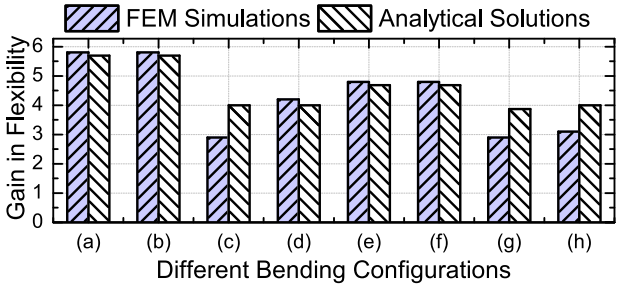

Fig. 12. Gain in flexibility for different bending axis presented in Fig. 10. (a), (b), (c), (d), (e), (f), (g), and (h) corresponds to various bending configurations in Fig. 10.

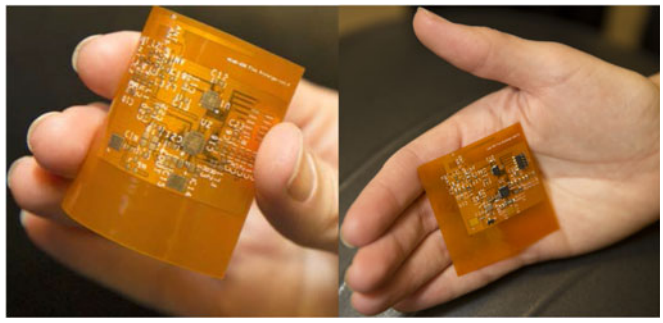

(a) Unmounted flexible bare board. (b) The prototype with all the chips mounted.

Fig. 13. The SoP prototype as bare board and with components mounted.

early proof-of-concept. We envision that FHE will be commonly used for designing wearable IoT devices. Therefore, our prototype integrates sensing, processing and wireless communication in a form factor that can fit in one's palm. We chose motion tracking and processing as the driver application since it can be used in a wide range of applications, from fitness tracking to gesture recognition. The prototype can be attached to the sleeve of clothing or placed in the palm, as illustrated in Fig. 13.

The complete list of components used in the prototype is provided in Table 2. The flexible Polyimide substrate used in our prototype has several advantages compared to a rigid FR-4 substrate. The flexible substrate is lighter, thinner, and can enable integration into wearable systems, such as electronics shirts, wrist bands, and electronic labels. To implement our driver application, we used a Motion Processing Unit (MPU) [26] that integrates accelerometer and gyroscope sensors built on micro-electromechanical systems (MEMS) technology. We chose a rigid MPU in our prototype mainly due to its size advantage. In general, sensing is one of the most promising subsystems that can be fully flexible. The sensor data in the MPU is first digitized using an ADC. Then, it is transmitted to a TI CC2650 MCU [53] via serial interface, such as I2C and SPI [33]. In general, powerful rigid chips are best suited to satisfy the performance requirements of processing tasks like gesture generation within a small footprint. However, flexible MCUs have also started to emerge as an alternative [1], albeit with lower computational capabilities. Our prototype transmits the processed data wirelessly to a smartphone using a Bluetooth Low Energy (BLE) interface [19] and a flexible inverted-F antenna. As presented later in Section 5.2, this antenna actually enables data transmission with the same performance as a rigid antenna. However, the rigid one would have decreased the flexibility of the SoP prototype. Therefore, the flexible antenna is a better choice since it provides the same performance with more flexibility. Finally, a custom smartphone application enables to visualize the motion of the prototype.

We performed extensive FEM simulations to evaluate different placement options for our prototype. In particular, we report simulation results for three scenarios:

1) The rigid chips are packed as densely as possible into a bounding-box. Then, the bounding-box is placed on one of the corners. This corresponds to the solution recommended by the proposed placement algorithm, which is also adapted in the current prototype;
2) The bounding-box is placed on the center of the substrate. This scenario enables quantitative comparison of the flexibility gain to the analytical results reported in Table 1;
3) The rigid chips are placed sparsely to facilitate wire routing instead of placement.

The recommended placement leads to $2.1\times$ gain in flexibility compared to placing the bounding-box on the center, which is aligned with the analytical results. Furthermore, the optimal solution gives $4.2\times$ better flexibility than the sparse placement. This result validates our choice of packing the rigid chips as densely as possible. In summary, FEM

TABLE 2
Summary of Components in the SoP Prototype

Type	Components	Total no of components	Total area (mm^2)
Rigid	Microcontroller (CC2650F128RSM)	1	16
	Motion Processing Unit (MPU9250)	1	9
	Oscillator1 (32.768 kHz)	1	4.8
	Oscillator2 (24 MHz)	1	8
	Voltage regulator	1	7.5
	Passive elements	41	3.48
Semi-Flexible	Copper plane + Antenna	1	1,332.51
Flexible	Polyimide substrate	1	2,500
Debug circuits	JTAG header	1	45.72
	Power test points	2	26.98

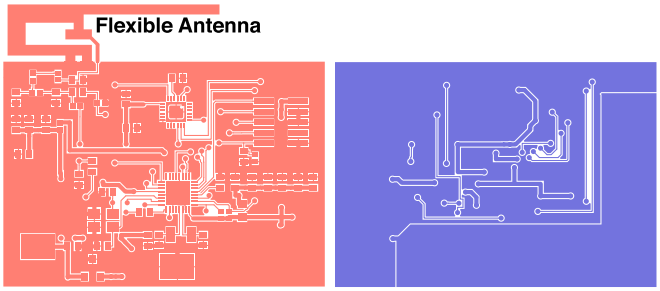

(a) Top layer. (b) Bottom layer.

Fig. 14. SoP prototype top and bottom layouts.

simulations confirm the optimality of placing the smallest possible bounding-box on one corner, which is a direct result of our placement methodology.

The optimized PCB layouts of the top and bottom layers of the bounding-box in the prototype are shown in Figs. 14a and 14b, respectively. We emphasize that the JTAG interface and debugging circuitry were added to facilitate debugging and programming. Therefore, the size of a product version of this prototype can be reduced by more than 50 percent.

5.1 SoP Prototype Characteristics

The characteristics of the prototype are summarized in Table 3. The prototype can transmit up to 192 kbps to the host computer, but we set the sampling period as 100 ms to minimize the energy consumption. This makes the transmission throughput as 1.44 kbps. The power consumption measured using Monsoon power meter [35] was 12.21 mW, which lead to 9.54 μJ of energy consumption to send one bit. The runtime power statistics of the SoP prototype according to the operating mode are summarized in Table 4. The experimental prototype was powered by an external source. However, we plan to use flexible batteries mounted on the bottom layer of the SoP. We expect about a 40 hour lifetime with continuous use when we employ a 130 mAh flexible battery [41].

5.2 Flexible Antenna Experiments

Bending may cause variation in the properties of the flexible components on the SoP, such as a flexible antenna.

TABLE 3
Characteristics of the SoP Prototype

Maximum performance	Operating performance	Connection interval	Energy/Tx
192 kbps	1.44 kbps	100 ms	9.54 μJ/bit

TABLE 4
Average Power Measurement Summary During Different Operating Modes of the SoP Prototype

Power consumption	Idle	Advertising	Connected idle	Tx sensor data
Peak (mW)	–	30.17	–	29.73
Average (mW)	3.59	4.27	3.60	12.21

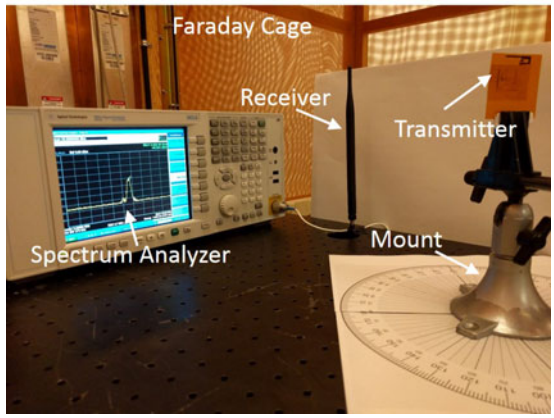

Fig. 15. Experimental setup for antenna measurements.

For example, the return loss of flexible antennas, such as a bow-tie antenna, can increase with bending [15]. To minimize the impact of bending, we employed an omnidirectional 2.4 GHz inverted-F antenna in our FHE prototype, as shown in Fig. 14a. In order to analyze the radiation characteristics of an antenna, i.e., to see whether it has an omnidirectional radiation pattern, it is important to plot the radiation pattern along 360 degrees. Changing the angle between the transmitter and receiver enables us to get the radiation patterns. To evaluate the antenna properties under different bending scenarios, we performed experiments inside a Faraday cage shown in Fig. 15.

First, we confirmed that the center frequency of the antenna remains constant, irrespective of bending. This is expected since bending does not affect the antenna dimensions. Then, we analyzed the received signal power as a function of bending when the receiver was 1 m away from the transmitter. In particular, we measured the received signal power when the prototype was flat and bent along 1.5 and 2 cm radii of curvature. We also repeated the measurement for inwards and outwards bending, as illustrated in Figs. 16a and 17a. Fig. 16b shows that the received power was affected significantly by inwards bending. For example, the received power decreased by as much as 5 dB when the angle (θ) between the transmitter and the receiver varied from 0 to 180 degree. This is roughly equivalent to increasing the separation between the transmitter and receiver by 2.5×. At the same time, the received signal power increased at certain angles, such as 60 degree. We conclude that the change in the received power stems primarily from multiple scattering due to electronic components on the interior side of the prototype. As a result, mostly destructive but also occasional constructive interference occurs at the receiving monopole antenna. This conclusion is supported by the results obtained for *outward* bending, as shown in Fig. 17b. Outward bending caused significantly smaller interference, and lead to significantly smaller variation due to bending. Fig. 17b also clearly demonstrates the omni-directional nature of the inverted-F antenna. In summary, this study shows that (a) bending may have intricate implications despite designing the antenna carefully, (b) inverted-F antenna can be a promising solution for flexible systems.

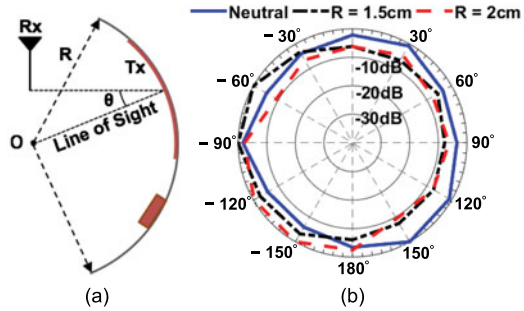

Fig. 16. (a) Illustration of inward bending. (b) Normalized radiation patterns of the flat and inward bent board.

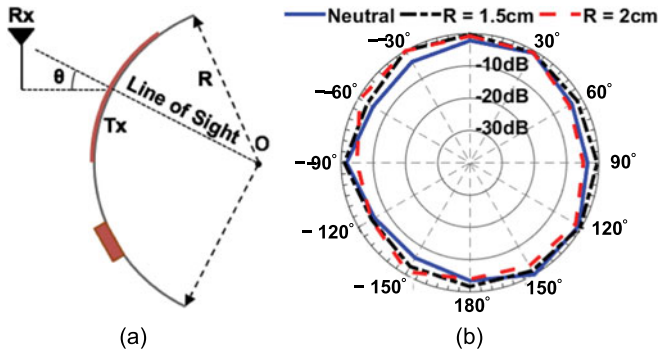

Fig. 17. (a) Illustration of outward bending. (b) Normalized radiation patterns of the flat and outward bent board.

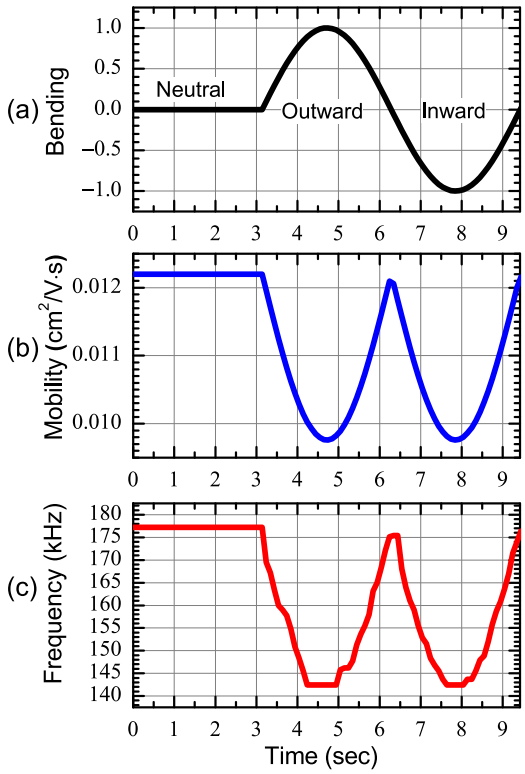

Fig. 19. The change in ring oscillator frequency because of change in mobility due to bending.

6 FHE Design Challenges and Future Research Directions

Here, we overview major challenges in the design of SoP architectures, and discuss potential research directions.

SoP Communication Challenges. A flexible circuit can be bent into several millimeter radius before creating strain-induce damage to the circuits. Bending the substrate can change the electron mobility by as much as 20 percent, and affect the timing of flexible circuits [42]. Moreover, physical changes in the substrate affect the interconnect capacitance, leading to further timing uncertainties. To analyze the effect of bending on flexible circuits, we first designed Pseudo-E CMOS type [24] inverter using IGZO TFT technology [39], as shown in Fig. 18a. We chose Pseudo-E CMOS inverters, since IGZO TFT technology supports only n-type transistors. Then, we implemented a ring oscillator given in Fig. 18b using the Pseudo-E CMOS inverters. Simulations using the SPICE tool showed a nominal operating frequency of 175 kHz for this circuit. Then, we emulated the bending scenario described in Fig. 19a by modulating the mobility. Initially, the mobility remained constant (labeled as Neutral in Fig. 19a). Next, the mobility decreased following a sine wave pattern to emulate outward and inward bending consecutively, as illustrated in Fig. 19b. As the mobility varied, we analyzed the output frequency of the ring oscillator. Fig. 19c shows the variation in the ring oscillator frequency with bending. When there was no bending (Neutral position), the ring oscillator frequency was measured as 175 kHz. As the circuit was bent, the carrier mobility decreased, leading to longer inverter propagation delay. The longer delay, in turn, decreased the ring oscillator frequency, as illustrated in Fig. 19c. In particular, the lowest frequency, observed at the maximum bending point, was recorded as 142 kHz.

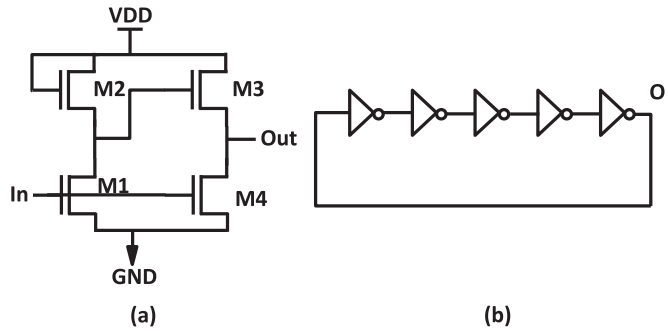

Fig. 18. (a) Design of basic pseudo-E CMOS inverter [24]. The W/L ratio used in this paper for M3 is $9\mu m/9\mu m$ and for all other transistors is $18\mu m/9\mu m$. (b) The circuit diagram of a ring oscillator made using pseudo-E CMOS inverters.

We also performed statistical analysis of the variation in the ring oscillator frequency by changing the mobility of the transistors. In particular, we performed Monte Carlo simulations to validate our bending approximation by varying the mobility using a Gaussian distribution with mean 0.012 $\mathrm{cm}^2/\mathrm{V}\cdot\mathrm{s}$ and standard deviation 20 percent. Each new sample of the transistor's mobility drawn from the distribution led to the change in inverter delays. Unlike the change in mobility of the transistors in Fig. 19b, the mobility in this experiment did not always change with the same value. We found that the variation in frequency generated by the ring oscillator was between 150 to 175 kHz, as shown in the Fig. 20. This frequency range is well within the bounds of the frequency shown in Fig. 19c. Note that we only showed the left arm of the Gaussian distribution in Fig. 20 since the overall effect of bending will lead to reduction in the mobility and therefore, performance.

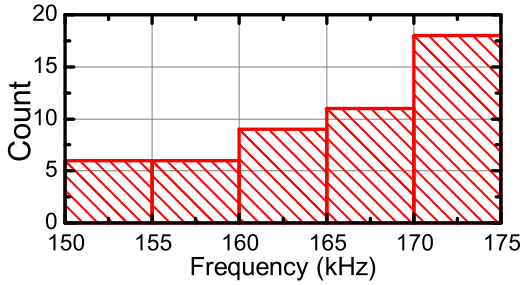

Fig. 20. Frequency histogram obtained by Monte Carlo simulation of the ring oscillator for 20 percent change in mobility.

Since the bending axis and amount of bending cannot be known a priori, the changes in timing and clock period of printed circuits are unpredictable. Consider the circuit in Fig. 21, which shows a combinational path between two registers. Bending can lead to setup and hold time violations as a function of the changes both in the delay of clock and combinational path. Designing for the worst case would deteriorate the performance, which is already suffering from low speeds and large feature sizes compared to the silicon chips. Furthermore, techniques proposed to improve the reliability by dynamically detecting timing violations have also limited applicability since they would also be affected by bending. For example, we implemented the slack-probe technique [31] using TFTs to cope with timing variations. Our simulations showed that the circuit can hardly reach 500 Hz.

Timing and synchronization in flexible circuits are complicated by factors including supply voltage, thermal, parameter variations, and bending. Therefore, asynchronous, or globally asynchronous locally synchronous (GALS) [40] communication, and latency-insensitive design techniques [8], [11] are much better fit for SoP communication. GALS is particularly attractive since different synchronous rigid chips can communicate over a network composed of asynchronous routers [40].

Potential Research Directions. There are a number of interesting research directions related to FHE. Manufacturing solutions and I/O interfaces, especially for stretchable electronics, will be major drivers for practical FHE solutions. Related to this, reliability is a major concern at both the material and system levels since FHE systems are subject to continuous physical deformation. For example, the drain current of the ultra-flexible pentacene FETs changes by about 10 percent after 160,000 bending cycles [42]. Since neither active cooling nor large heat sinks can be used on flexible substrates, novel thermal and power management techniques targeting SoPs are needed. Finally, security and privacy will be important considerations as FHE systems are expected to collect and process personal data.

7 Conclusion

This paper introduced SoP architectures, a new hybrid approach to implementing electronics on flexible substrates. By combining the advantages of flexible electronics and silicon technology, SoP architectures offer great potential in transforming wearable computing systems. However, there are many design and technology challenges in adapting these novel architectures. As the first step in addressing these challenges, we introduced flexibility as a new metric,

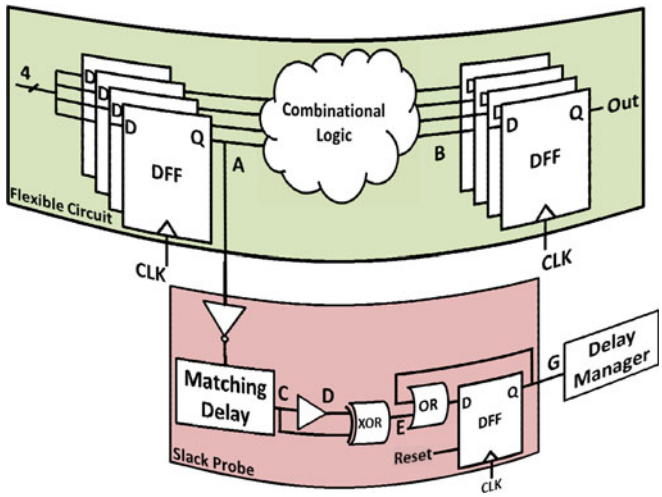

Fig. 21. Flexible circuit pipeline showing four input and four output registers with combinational logic. A slack-probe [31] has been inserted at point A, to detect delay failure.

in addition to traditional power, area and performance metrics. Using this new metric, we developed a methodology for the optimal placement of rigid chips on flexible substrates to maximize flexibility. The optimal placements showed 5.7× enhancement in flexibility compared to a naïve placement. Finally, we validated the optimization scenarios through FEM simulations, and we presented a SoP prototype targeting sensing applications.

Appendix

In this section, we present the proof of Theorem 1 which specifies the optimal placement along one dimension.

Proof of Part 1. Consider the flexibility of non-overlapping chips given by Equation (4)

$$\delta(\boldsymbol{x}) = \frac{P_{\max}}{3EI}\left[x_1^3 + \sum_{i=1}^{N-1}(x_{i+1} - (x_i + l_i))^3 + (L - (x_N + l_N))^3\right].$$

Derivative w.r.t. x_1. The first and second order analytical derivatives of Equation (4) w.r.t. x_1 are

$$\frac{\partial\delta(\boldsymbol{x})}{\partial x_1} = \frac{P_{\max}}{3EI}\left[3x_1^2 - 3(x_2 - x_1 - l_1)^2\right] \tag{18}$$

$$\frac{\partial^2\delta(\boldsymbol{x})}{\partial x_1^2} = \frac{P_{\max}}{3EI}\left[6x_1 + 6(x_2 - x_1 - l_1)\right]. \tag{19}$$

Since $0 \le x_1 \le x_2 - l_1$, the second order derivative in Equation (19) is non-negative. This implies that the first order derivative $\frac{\partial\delta(\boldsymbol{x})}{\partial x_1}$ is non-decreasing. The first order derivatives at the boundaries of x_1 can be written as

$$\left.\frac{\partial\delta(\boldsymbol{x})}{\partial x_1}\right|_{x_1=0} = \frac{P_{\max}}{3EI}\left[-3(x_2 - l_1)^2\right] \le 0 \tag{20}$$

$$\left.\frac{\partial\delta(\boldsymbol{x})}{\partial x_1}\right|_{x_1=x_2-l_1} = \frac{P_{\max}}{3EI}\left[3(x_2 - l_1)^2\right] \ge 0. \tag{21}$$

Equation (20) implies that $\delta(\boldsymbol{x})$ is decreasing or flat at $x_1 = 0$, while Equation (21) implies that $\delta(\boldsymbol{x})$ is increasing

or constant at $x_1 = x_2 - l_1$. Since the first order derivative is non-decreasing, the flexibility $\delta(\boldsymbol{x})$ has to be maximum at one of the boundaries $x_1 = 0$ or $x_1 = x_2 - l_1$.

Derivative w.r.t. x_i. The first and second order derivatives w.r.t. x_i, for $1 < i < N$ can be written as

$$\frac{\partial \delta(\boldsymbol{x})}{\partial x_i} = \frac{P_{\max}}{3EI}\left[3(x_i - x_{i-1} - l_{i-1})^2 - 3(x_{i+1} - x_i - l_i)^2\right] \tag{22}$$

$$\frac{\partial^2 \delta(\boldsymbol{x})}{\partial x_i^2} = \frac{P_{\max}}{3EI}\left[6(x_i - x_{i-1} - l_{i-1}) + 6(x_{i+1} - x_i - l_i)\right]. \tag{23}$$

Since $x_{i-1} + l_{i-1} \le x_i \le x_{i+1} - l_i$, the derivative $\frac{\partial^2 \delta(\boldsymbol{x})}{\partial x_i^2}$ is non-negative, which implies the first order derivative $\frac{\partial \delta(\boldsymbol{x})}{\partial x_i}$ is non-decreasing. Furthermore, the first order derivative at the lower and higher boundaries of x_i can be written as

$$\left.\frac{\partial \delta(\boldsymbol{x})}{\partial x_i}\right|_{x_i = x_{i-1} + l_{i-1}} = \frac{P_{\max}}{3EI}\left[-3(x_{i+1} - x_{i-1} - l_{i-1} - l_i)^2\right] \le 0 \tag{24}$$

$$\left.\frac{\partial \delta(\boldsymbol{x})}{\partial x_i}\right|_{x_i = x_{i+1} - l_i} = \frac{P_{\max}}{3EI}\left[3(x_{i+1} - l_i - x_{i-1} - l_{i-1})^2\right] \ge 0. \tag{25}$$

Again, $\delta(\boldsymbol{x})$ is decreasing or flat at the lower bound, and it is increasing or flat at the upper bound. Since the first order derivative is non-decreasing, the flexibility $\delta(\boldsymbol{x})$ has to be maximum at one of the boundaries.

Derivative w.r.t. x_N. The first and second order derivatives w.r.t. x_N can be written as

$$\frac{\partial \delta(\boldsymbol{x})}{\partial x_N} = \frac{P_{\max}}{3EI}\left[3(x_N - x_{N-1} - l_{N-1})^2 - 3(L - x_N - l_N)^2\right] \tag{26}$$

$$\frac{\partial^2 \delta(\boldsymbol{x})}{\partial x_N^2} = \frac{P_{\max}}{3EI}\left[6(x_N - x_{N-1} - l_{N-1}) + 6(L - x_N - l_N)\right]. \tag{27}$$

Since $x_{N-1} + l_{N-1} \le x_N \le L - l_N$, the derivative $\frac{\partial^2 \delta(\boldsymbol{x})}{\partial x_N^2}$ is non-negative, which implies the first order derivative $\frac{\partial \delta(\boldsymbol{x})}{\partial x_N}$ is non-decreasing. Furthermore, the first order derivative at the lower and upper bounds of x_N can be written as

$$\left.\frac{\partial \delta(\boldsymbol{x})}{\partial x_N}\right|_{x_N = x_{N-1} + l_{N-1}} = \frac{P_{\max}}{3EI}\left[-3(L - x_{N-1} - l_{N-1} - l_N)^2\right] \le 0 \tag{28}$$

$$\left.\frac{\partial \delta(\boldsymbol{x})}{\partial x_N}\right|_{x_N = L - l_N} = \frac{P_{\max}}{3EI}\left[3(L - l_N - x_{N-1} - l_{N-1})^2\right] \ge 0. \tag{29}$$

By the same token, the flexibility $\delta(\boldsymbol{x})$ has to be maximum on one of the boundaries, $x_N = x_{N-1} + l_{N-1}$ or $x_N = L - l_N$. As a result, the flexibility is maximized when all the chips are placed side by side (i.e., they form a contiguous region) on either side of the substrate.

A particular optimal solution instance is $x_1 = 0$ and $x_i = x_{i-1} + l_{i-1}$ for $2 \le i \le N$. The maximum displacement in this case evaluates to

$$\delta_{\text{nonoverlapping}} = \frac{P_{\max}}{3EI}\left(L - \sum_{i=1}^{N} l_i\right)^3 \tag{30}$$

□

Proof of Part 2. Consider the maximum deflection of overlapping chips given by Equation (6)

$$\delta(x_1, \boldsymbol{o}) = \frac{P_{\max}}{3EI}\left[x_1^3 + \left(L - \left(x_1 + \sum_{i=1}^{N} l_i - \sum_{i=1}^{N-1} o_i\right)\right)^3\right].$$

Derivative w.r.t. x_1. The first and second order derivatives of Equation (6) w.r.t. x_1 are

$$\frac{\partial \delta(x_1, \boldsymbol{o})}{\partial x_1} = \frac{P_{\max}}{3EI}\left[3x_1^2 - 3\left(L - x_1 - \sum_{i=1}^{N} l_i + \sum_{i=1}^{N-1} o_i\right)^2\right] \tag{31}$$

$$\frac{\partial^2 \delta(x_1, \boldsymbol{o})}{\partial x_1^2} = \frac{P_{\max}}{3EI}\left[6x_1 + 6\left(L - x_1 - \sum_{i=1}^{N} l_i + \sum_{i=1}^{N-1} o_i\right)\right]. \tag{32}$$

Since $0 \le x_1 \le L - l_1$ and the substrate length is large enough to accommodate all the chips, i.e., $L \ge x_1 + \sum_{i=1}^{N} l_i - \sum_{i=1}^{N-1} o_i$, the second order derivative $\frac{\partial^2 \delta(x_1, \boldsymbol{o})}{\partial x_1^2}$ is non-negative. This implies the first order derivative $\frac{\partial \delta(x_1, \boldsymbol{o})}{\partial x_1}$ is either increasing or flat. Furthermore, the first order derivative at the lower and higher boundaries of x_1 can be written as

$$\left.\frac{\partial \delta(x_1, \boldsymbol{o})}{\partial x_1}\right|_{x_1 = 0} = \frac{P_{\max}}{3EI}\left[-3\left(L - \sum_{i=1}^{N} l_i + \sum_{i=1}^{N-1} o_i\right)^2\right] \le 0 \tag{33}$$

$$\left.\frac{\partial \delta(x_1, \boldsymbol{o})}{\partial x_1}\right|_{x_1 = L - l_1} = \frac{P_{\max}}{3EI}\left[3(L - l_1)^2 - 3\left(\left(\sum_{i=1}^{N} l_i - \sum_{i=1}^{N-1} o_i\right) - l_1\right)^2\right] \ge 0. \tag{34}$$

At $x_1 = 0$, the first order derivative is negative. At $x_1 = L - l_1$, the first order derivative is positive because $L > \sum_{i=1}^{N} l_i - \sum_{i=1}^{N-1} o_i$. Equation (33) implies that $\delta(x_1, \boldsymbol{o})$ is decreasing or flat at $x_1 = 0$, while Equation (34) implies that $\delta(x_1, \boldsymbol{o})$ is increasing or constant at $x_1 = L - l_1$. Since the first order derivative is non-decreasing, the flexibility $\delta(x_1, \boldsymbol{o})$ has to be maximum at one of the boundaries $x_1 = 0$ or $x_1 = L - l_1$.

Derivative w.r.t. o_i. The first order derivative of the Equation (6) w.r.t. the overlap o_i can be written as

$$\frac{\partial \delta(x_1, \boldsymbol{o})}{\partial o_i} = \frac{P_{\max}}{3EI}\left[3\left(L - x_1 - \sum_{i=1}^{N} l_i + \sum_{i=1}^{N-1} o_i\right)^2\right] \ge 0. \tag{35}$$

Since the first order partial derivative w.r.t. o_i is non-negative, the flexibility $\delta(x_1, \boldsymbol{o})$ is either increasing or flat. Therefore, the maximum value of $\delta(x_1, \boldsymbol{o})$ for a given x_1 occurs, when the overlaps (o_i) are maximum. Since $0 \leq o_i \leq \min(l_i, l_{i+1}), \forall\ 1 \leq i < N$, the sum $\sum_{i=1}^{N-1} o_i$ reaches its maximum value when each of the o_i is maximum. As a result, the flexibility is maximized if the chips are placed on either side, and the overlap between each pair is *maximum*.

A particular optimal solution instance is $x_1 = 0$ and $o_i = \min(l_i, l_{i+1})$ for $1 \leq l < N$. To plug these values to Equation (6), we need to compute the sum of the overlaps $\sum_i o_i$. We achieve this as follows:

$$\sum_{i=1}^{N-1} \max(o_i) = \sum_{i=1}^{N-1} \min(l_i, l_{i+1}) = \sum_{i=1}^{N} l_i - \max_{1 \leq i \leq N} l_i.$$

The first equality in this equation follows directly from the upper bound of o_i. The second equality reflects the fact that the summation term $\sum_{i=1}^{N-1} \min(l_i, l_{i+1})$ evaluates to the sum of the lengths of all rigid components excluding the length of the longest chip. When we plug the last expression and $x_1 = 0$ to Equation (6), we obtain the maximum flexibility with overlap as

$$\begin{aligned}
\delta_{\text{overlapping}} &= \frac{P_{\max}}{3EI}\left[L - \sum_{i=1}^{N} l_i + \sum_{i=1}^{N-1} \max(o_i)\right]^3 \\
\delta_{\text{overlapping}} &= \frac{P_{\max}}{3EI}\left[L - \sum_{i=1}^{N} l_i + \sum_{i=1}^{N} l_i - \max_{1 \leq i \leq N} l_i\right]^3 \qquad (36) \\
\delta_{\text{overlapping}} &= \frac{P_{\max}}{3EI}\left[L - \max_{1 \leq i \leq N} l_i\right]^3
\end{aligned}$$

□

ACKNOWLEDGMENTS

This work was supported by the NSF CAREER Program. The authors thank Mohit Parihar and Shankhadeep Mukerji of the Arizona State University for their help in building the SoP prototype. The authors also thank the anonymous reviewers for their insightful comments that improved the original manuscript tremendously.

REFERENCES

[1] American Semiconductor Inc., "FleX Silicon-on-Polymer, FleX-MCU, FleX-RFIC, FleX-ADC," (2016). [Online]. Available: http://www.americansemi.com
[2] S. N. Adya and I. L. Markov, "Fixed-outline floorplanning: Enabling hierarchical design," *IEEE Trans. Very Large Scale Integr.*, vol. 11, no. 6, pp. 1120–1135, Dec. 2003.
[3] Arubixs, "Portal—Flexible Wearable Smartphone," (2016). [Online]. Available: https://www.indiegogo.com/projects/portal-by-arubixs-flexible-wearable-smartphone
[4] M. F. Ashby, *Materials Selection in Mechanical Design*, 4th ed. London, U.K.: Butterworth-Heinemann, 2011.
[5] ASU, "Flexible Display Center," (2016). [Online]. Available: https://flexdisplay.asu.edu/
[6] S. Boyd and L. Vandenberghe, *Convex Optimization*. Cambridge, U.K.: Cambridge Univ. Press, 2004.
[7] Q. Cao, et al., "Medium-scale carbon nanotube thin-film integrated circuits on flexible plastic substrates," *Nature*, vol. 454, no. 7203, pp. 495–500, 2008.
[8] L. P. Carloni, K. L. McMillan, and A. L. Sangiovanni-Vincentelli, "Theory of latency-insensitive design," *IEEE Trans. Comput.-Aided Des. Integr. Circuits Syst.*, vol. 20, no. 9, pp. 1059–1076, Nov. 2001.
[9] R. L. Chaney, et al., "FleX silicon-on-polymer: Flexible (pliable) ICs from commercial foundry processes," in *Proc. Government Microcircuit Appl. Critical Technol. Conf.*, Mar. 2013.
[10] *Comsol Multiphysics User's Guide, Version: 5.1*, Comsol, Stockholm, Sweden, 2015.
[11] J. Cortadella and M. Kishinevsky, "Synchronous elastic circuits with early evaluation and token counterflow," in *Proc. Des. Autom. Conf.*, 2007, pp. 416–419.
[12] B. Crone, et al., "Large-scale complementary integrated circuits based on organic transistors," *Nature*, vol. 403, no. 6769, pp. 521–523, 2000.
[13] C. Drury, et al., "Low-cost all-polymer integrated circuits," *Appl. Phys. Lett.*, vol. 73, no. 1, pp. 108–110, 1998.
[14] Dupont, "Flexible Circuit Materials," (2016). [Online]. Available: http://www.dupont.com/
[15] A. C. Durgun, C. A. Balanis, C. R. Birtcher, and D. R. Allee, "Design, simulation, fabrication and testing of flexible bow-tie antennas," *IEEE Trans. Antennas Propag.*, vol. 59, no. 12, pp. 4425–4435, Dec. 2011.
[16] H. Ebihara, et al., "P-39: A flexible 16kb SRAM based on low-temperature poly-silicon (LTPS) TFT technology," *SID Symp. Dig. Tech. Papers*, vol. 37, no. 1, pp. 339–342, 2006.
[17] M. Escalante, A. B. Kahng, M. Kishinevsky, U. Ogras, and K. Samadi, "Multi-product floorplan and uncore design framework for chip multiprocessors," in *Proc. Int. Workshop Syst. Level Interconnect Prediction*, 2015, pp. 1–7.
[18] R. Ganesan, J. Krumm, S. Pankalla, K. Ludwig, and M. Glesner, "Design of an organic electronic label on a flexible substrate for temperature sensing," in *Proc. IEEE ESSCIRC*, 2013, pp. 423–426.
[19] C. Gomez, J. Oller, and J. Paradells, "Overview and evaluation of bluetooth low energy: An emerging low-power wireless technology," *Sensors*, vol. 12, no. 9, pp. 11734–11753, 2012.
[20] S. Gowrisanker, et al., "A novel low temperature integration of hybrid CMOS devices on flexible substrates," *Organic Electron.*, vol. 10, no. 7, pp. 1217–1222, 2009.
[21] U. Gupta, S. Jain, and U. Y. Ogras, "Can systems extended to polymer? SoP architecture design and challenges," in *Proc. Int. Syst.-on-Chip Conf.*, Sep. 2015, pp. 203–208.
[22] Y. Hu, et al., "A self-powered system for large-scale strain sensing by combining CMOS ICs with large-area electronics," *IEEE J. Solid-State Circuits*, vol. 49, no. 4, pp. 838–850, Apr. 2014.
[23] T.-C. Huang, J.-L. Huang, and K.-T. Cheng, "Robust circuit design for flexible electronics," *IEEE Des. Test Comput.*, vol. 28, no. 6, pp. 8–15, Nov./Dec. 2011.
[24] T.-C. Huang, et al., "Pseudo-CMOS: A novel design style for flexible electronics," in *Proc. Conf. Des. Autom. Test Europe*, 2010, pp. 154–159.
[25] T.-C. J. Huang, et al., "Design, automation, and test for low-power and reliable flexible electronics," *Found. Trends Electron. Des. Autom.*, vol. 9, no. 2, pp. 99–210, 2015.
[26] InvenSense Inc., "MPU-9250," (2016). [Online]. Available: www.invensense.com/
[27] S. Jacob, et al., "High performance printed N and P-type OTFTs enabling digital and analog complementary circuits on flexible plastic substrate," *Solid-State Electron.*, vol. 84, pp. 167–178, 2013.
[28] N. Karaki, et al., "43.1: A flexible 8-bit asynchronous microprocessor based on low-temperature poly-silicon (LTPS) TFT technology," *SID Symp. Dig. Tech. Papers*, vol. 36, no. 1, pp. 1430–1433, 2005.
[29] H. E. Katz and J. Huang, "Thin-film organic electronic devices," *Annu. Rev. Mater. Res.*, vol. 39, pp. 71–92, 2009.
[30] M. Koo, et al., "Bendable inorganic thin-film battery for fully flexible electronic systems," *Nano Lett.*, vol. 12, no. 9, pp. 4810–4816, 2012.
[31] L. Lai, V. Chandra, R. Aitken, and P. Gupta, "SlackProbe: A low overhead in situ on-line timing slack monitoring methodology," in *Proc. Conf. Des. Autom. Test Europe*, 2013, pp. 282–287.
[32] H. G. Lee and N. Chang, "Powering the IoT: Storage-less and converter-less energy harvesting," in *Proc. IEEE 20th Asia South Pacific Des. Autom. Conf.*, 2015, pp. 124–129.
[33] F. Leens, "An introduction to I2C and SPI protocols," *Instrum. Meas. Mag.*, vol. 12, no. 1, pp. 8–13, 2009.
[34] J.-L. Lin, P.-H. Wu, and T.-Y. Ho, "Placement optimization of flexible TFT circuits with mechanical strain and temperature consideration," *ACM J. Emerg. Technol. Comput. Syst.*, vol. 11, no. 1, 2014, Art. no. 1.

[35] Monsoon Solutions Inc., "Monsoon Power Meter," (2016). [Online]. Available: https://www.msoon.com/LabEquipment/PowerMonitor/
[36] T. Moy, et al., "Thin-film circuits for scalable interfacing between large-area electronics and CMOS ICs," in *Proc. Device Res. Conf.*, 2014, pp. 271–272.
[37] A. Nathan, et al., "Flexible electronics: The next ubiquitous platform," *Proc. IEEE*, vol. 100, no. special centennial issue, pp. 1486–1517, May 2012.
[38] J. Noh, M. Jung, Y. Jung, C. Yeom, M. Pyo, and G. Cho, "Key issues with printed flexible thin film transistors and their application in disposable RF sensors," *Proc. IEEE*, vol. 103, no. 4, pp. 554–566, Apr. 2015.
[39] K. Nomura, et al., "Room-temperature fabrication of transparent flexible thin-film transistors using amorphous oxide semiconductors," *Nature*, vol. 432, no. 7016, pp. 488–492, 2004.
[40] S. Nowick and M. Singh, "Asynchronous design part 1: Overview and recent advances," *IEEE Des. Test*, vol. 32, no. 3, pp. 5–18, Jun. 2015.
[41] PowerStream Technology, "Ultrathin Rechargeable Lithium Polymer Batteries," (2016). [Online]. Available: http://www.powerstream.com/thin-lithium-ion.htm
[42] T. Sekitani, et al., "Ultraflexible organic field-effect transistors embedded at a neutral strain position," *Appl. Phys. Lett.*, vol. 87, no. 17, 2005, Art. no. 173502.
[43] J. Sheats, "Truly wearable electronics," in *Proc. FlexTech Alliance Workshop: Flexible Hybrid Electron. Challenges Solutions*, Jul. 2014.
[44] J. Smith, et al., "Application of flexible flat panel display technology to wearable biomedical devices," *Electron. Lett.*, vol. 51, no. 17, pp. 1312–1314, 2015.
[45] J. T. Smith, B. O'Brien, Y.-K. Lee, E. J. Bawolek, and J. B. Christen, "Application of flexible OLED display technology for electro-optical stimulation and/or silencing of neural activity," *J. Display Technol.*, vol. 10, no. 6, pp. 514–520, 2014.
[46] T. Someya, et al., "Conformable, flexible, large-area networks of pressure and thermal sensors with organic transistor active matrixes," *Proc. Nat. Academy Sci. USA*, vol. 102, no. 35, pp. 12321–12325, 2005.
[47] A. Sou, et al., "Programmable logic circuits for functional integrated smart plastic systems," *Organic Electron.*, vol. 15, no. 11, pp. 3111–3119, 2014.
[48] R. Street, et al., "From printed transistors to printed smart systems," *Proc. IEEE*, vol. 103, no. 4, pp. 607–618, Apr. 2015.
[49] World Technology Evaluation Center, Inc. (WTEC), "WTEC Workshop on International R&D in Flexible Hybrid Electronics," Jun. 2009. [Online]. Available: http://www.wtec.org/flex/, Accessed on: 22 Jun. 2015.
[50] D.-m. Sun, et al., "Flexible high-performance carbon nanotube integrated circuits," *Nature Nanotechnol.*, vol. 6, no. 3, pp. 156–161, 2011.
[51] B. A. Szabo and I. Babuška, *Finite Element Analysis*. Hoboken, NJ, USA: Wiley, 1991.
[52] R. Tarjan, "Depth-first search and linear graph algorithms," *SIAM J. Comput.*, vol. 1, no. 2, pp. 146–160, 1972.
[53] Texas Instruments Inc., "CC-2650 Microcontroller," (2016). [Online]. Available: http://www.ti.com/product/CC2650
[54] S. Tokito, et al., "15.1: Invited paper: Printed organic TFT array and integrated circuits," *SID Symp. Dig. Tech. Papers*, vol. 45, no. 1, pp. 180–182, 2014.
[55] J. Vaillancourt, et al., "All ink-jet-printed carbon nanotube thin-film transistor on a polyimide substrate with an ultrahigh operating frequency of over 5 GHz," *Appl. Phys. Lett.*, vol. 93, no. 24, 2008, Art. no. 243301.
[56] N. Watthanawisuth, T. Maturos, A. Sappat, and A. Tuantranont, "The IoT wearable stretch sensor using 3D-graphene foam," in *Proc. IEEE SENSORS*, 2015, pp. 1–4.
[57] B. Yoo, et al., "High-mobility bottom-contact n-channel organic transistors and their use in complementary ring oscillators," *App. Phys. Lett.*, vol. 88, no. 8, 2006, Art. no. 082104.
[58] F. Zhang, et al., "Polymer photovoltaic cells with conducting polymer anodes," *Adv. Mater.*, vol. 14, no. 9, pp. 662–665, 2002.

Ujjwal Gupta received the BE degree in electronics and communication engineering from Manipal University, Karnataka, India, in 2011, and the MS degree in electrical engineering from Arizona State University, Tempe, Arizona, in 2014. He is currently working toward the PhD degree in the Department of Electrical, Computer, and Energy Engineering, Arizona State University, Tempe. His research interests include dynamic power management and electronic design automation of multiprocessor systems-on-chip (MpSoC).

Jaehyun Park received the BS degree in electrical engineering and PhD degree in electrical engineering and computer science from Seoul National University, Seoul, Korea, in 2006 and 2015, respectively. From 2009 to 2010, he was a visiting scholar with the University of Southern California, Los Angeles, California. He is currently an exchange scholar in the School of Electrical, Computer and Energy Engineering, Arizona State University, Tempe, Arizona. His current research interests include flexible hybrid electronics, low-power embedded system design, and non-volatile memory system design.

Hitesh Joshi received the BTech degree in electronics & instrumentation engineering from UPTU, Lucknow, India. He is currently working toward the MS degree in electrical engineering at Arizona State University. His specialization is electronics and mixed signal circuit design. His research interests are related to embedded systems and flexible hybrid electronics (FHE).

Umit Y. Ogras received the PhD degree in electrical and computer engineering from Carnegie Mellon University, Pittsburgh, Pennsylvania, in 2007. From 2008 to 2013, he worked as a research scientist in the Strategic CAD Laboratories, Intel Corporation. He is currently an assistant professor with the School of Electrical, Computer and Energy Engineering. Recognitions he has received include the Strategic CAD Labs Research Award, 2012 IEEE Donald O. Pederson Transactions on CAD Best Paper Award, 2011 IEEE VLSI Transactions Best Paper Award, and 2008 EDAA Outstanding PhD Dissertation Award. His research interests include digital system design, embedded systems, multicore architecture, and electronic design automation with particular emphasis on multiprocessor systems-on-chip (MPSoC).